Reproducibility of Natural Shear Wave Elastography Measurements

Keijzer, Lana B.H.; Strachinaru, Mihai; Bowen, Dan J.; Geleijnse, Marcel L.; van der Steen, Antonius F.W.; Bosch, Johan G.; de Jong, Nico; Vos, Hendrik J.

DOI
10.1016/j.ultrasmedbio.2019.09.002

Publication date
2019

Document Version
Final published version

Published in
Ultrasound in Medicine and Biology

Ultrasound in Med. & Biol., Vol. 45, No. 12, pp. 3172–3185, 2019

0301-5629/$ - see front matter

https://doi.org/10.1016/j.ultrasmedbio.2019.09.002

● *Original Contribution*

REPRODUCIBILITY OF NATURAL SHEAR WAVE ELASTOGRAPHY MEASUREMENTS

Lana B.H. Keijzer,* Mihai Strachinaru,*,† Dan J. Bowen,† Marcel L. Geleijnse,† Antonius F.W. van der Steen,†,‡ Johan G. Bosch,† Nico de Jong,†,‡ and Hendrik J. Vos†,‡

* Biomedical Engineering, Thorax Center, Erasmus MC, Rotterdam, The Netherlands; † Cardiology, Thorax Center, Erasmus MC, Rotterdam, The Netherlands; and ‡ Acoustical Wavefield Imaging, ImPhys, Delft University of Technology, The Netherlands

(*Received* 15 *February* 2019; *revised* 30 *August* 2019; *in final from* 4 *September* 2019)

Abstract—For the quantification of myocardial function, myocardial stiffness can potentially be measured non-invasively using shear wave elastography. Clinical diagnosis requires high precision. In 10 healthy volunteers, we studied the reproducibility of the measurement of propagation speeds of shear waves induced by aortic and mitral valve closure (AVC, MVC). Inter-scan was slightly higher but in similar ranges as intra-scan variability (AVC: 0.67 m/s (interquartile range [IQR]: 0.40–0.86 m/s) versus 0.38 m/s (IQR: 0.26–0.68 m/s), MVC: 0.61 m/s (IQR: 0.26–0.94 m/s) versus 0.26 m/s (IQR: 0.15–0.46 m/s)). For AVC, the propagation speeds obtained on different day were not statistically different ($p = 0.13$). We observed different propagation speeds between 2 systems (AVC: 3.23–4.25 m/s [Zonare ZS3] versus 1.82–4.76 m/s [Philips iE33]), $p = 0.04$). No statistical difference was observed between observers (AVC: $p = 0.35$). Our results suggest that measurement inaccuracies dominate the variabilities measured among healthy volunteers. Therefore, measurement precision can be improved by averaging over multiple heartbeats. (E-mail: l.b.h.keijzer@erasmusmc.nl)

Key Words: **Shear waves, Elastography, Valve closure, stiffness, High frame rate, Natural shear wave elastography, Tissue elasticity imaging.**

INTRODUCTION

In developed countries, approximately 1%–2% of the adult population has heart failure. The prevalence is even rising to >10% among people older than 70 y (Ponikowski et al. 2016). Currently, geometric volumes and non-invasive Doppler measurements of tissue and blood are used for the echocardiographic evaluation of cardiac myocardial function (Lang et al. 2015; Nagueh et al. 2016). Nonetheless, these parameters that for the most part measure the effects of myocardial function are load dependent (Voigt 2019). No accurate method currently exists for non-invasive cardiac stiffness measurements. Measuring the stiffness of the myocardium likely provides more direct insights in the condition of the myocardium (Voigt 2019), as recently shown by Villemain et al. (2019) in a group of volunteers and hypertrophic cardiomyopathy patients using shear wave elastography measurements (SWE). To distinguish the types of diastolic and systolic dysfunctions and to accommodate more personalized treatments, non-invasive stiffness measurements could be a valuable tool.

Several studies have shown the potential of shear waves (SWs) to be used for measuring the stiffness of the myocardium non-invasively (Wassenaar et al. 2016; Arani et al. 2017a; Petrescu et al. 2019; Santos et al. 2019; Strachinaru et al. 2019; Villemain et al. 2019). The propagation speed of these SWs is expected to be linked to Young's modulus of the myocardium.

Magnetic resonance and ultrasound imaging have been used in a variety of animal and human studies to perform SWE measurements. The advantage of using magnetic resonance imaging (MRI) is that the 3-D displacement field of the SWs in the complex cardiac geometry can be measured (Arani et al. 2017b). However, MRI is expensive, uncomfortable and slow. Moreover, MRI cannot be used for patients with arrhythmia because of cardiac gating. For SWE using ultrasound imaging,

Address correspondence to: Lana B.H. Keijzer, Department of Biomedical Engineering, Thorax Center, Erasmus MC, Room Ee2302, PB 2040, 3000 CA Rotterdam, The Netherlands.
E-mail: l.b.h.keijzer@erasmusmc.nl

several studies have used external sources, such as mechanical shakers (Tzschätzsch et al. 2012; Urban et al. 2013; Pislaru et al. 2014b) or acoustic radiation forces (ARF) (Bouchard et al. 2009; Couade et al. 2011; Pernot et al. 2011; Hollender et al. 2012; Pernot et al. 2016; Song et al. 2016; Villemain et al. 2019) to induce SWs. The SWs naturally occurring after aortic valve closure (AVC) or mitral valve closure (MVC) have been investigated as well (Kanai 2005; Pernot et al. 2007; Brekke et al. 2014; Pislaru et al. 2014a; Vos et al. 2017; Santos et al. 2019; Strachinaru et al. 2019). An advantage of exploiting the SWs induced by valve closure is that these SWs were observed to have larger tissue velocity amplitudes (~40 mm/s) (Vos et al. 2017) than the SWs induced by an external acoustical force (~10 mm/s) (Couade et al. 2011), likely leading to higher signal-to-noise ratios. However, the low frequency content of natural SWs (Kanai 2005; Vos et al. 2017; Santos et al. 2019) compared with external sources (Couade et al. 2011; Hollender et al. 2012; Pislaru et al. 2014b), and thus the inherently larger wavelengths form a disadvantage of natural shear wave speed (SWS) measurements. Because the SWs can only be tracked over the limited length of a few centimeters of the interventricular septum (IVS), smaller fractions of the wavelength can be tracked for SWs with low frequencies, causing measurement inaccuracy. In addition, for 2-D natural SWS measurements, the source of the SWs is not ensured to be in the plane with the field of view, as is the case for ARF-based measurements, and therefore out-of-plane propagation could also induce measurement inaccuracy (Vos et al. 2017). These measurement inaccuracies should be minimized for clinical diagnoses where a high precision of the SWS measurements is needed.

Other than measurement inaccuracies, SWS measurements are expected to be affected by various phenomena. First, the myocardial stiffness measured depends on the intrinsic viscoelastic material characteristics of the myocardium, independent of loading conditions. Significant different propagation speeds have been measured after AVC and MVC for pathologic stiff myocardium as in hypertrophic cardiomyopathy (Strachinaru et al. 2019) and amyloidosis patients (Petrescu et al. 2019) compared with healthy volunteers. Second, the moment in the cardiac cycle will determine to what extent passive myocardial stiffness and additional myocardial contractility are measured. This is opposite to the alternative method of using ARF to induce SWs, as the ARF push can be timed throughout the cardiac cycle and hence is able to capture the myocardium in a relaxed state. The variations in myocardial stiffness during the cardiac cycle have been measured in several studies (Couade et al. 2011; Hollender et al. 2017). However, SWs induced by valve closure only occur at two stages of the cardiac cycle, during which the heart is not completely relaxed. Therefore, natural SWS measurements most likely measure a combination of passive myocardial stiffness and contractility, potentially providing information about diastolic and systolic function, albeit that the disentangling is a challenge. Third, because of the nonlinear stress-strain relationship of biologic materials (Mirsky and Parmley 1973), the filling state of the ventricle is still expected to influence SWS measurements, even when measured at end-diastole (Voigt 2019). Furthermore, contractility is also known to be affected by pre-load *via* the Frank-Starling mechanism. Therefore, other than measurement inaccuracies, hemodynamic variations are also expected to affect reproducibility.

For the application of clinical diagnosis, knowledge on measurement reproducibility is needed to distinguish normal and pathologic myocardial function. This study tests the reproducibility of determining the propagation speed of natural SWs induced in the IVS by AVC and MVC in healthy volunteers. Studies have shown that propagation speeds after AVC can be determined *in vivo* by using a clinical ultrasound system using conventional or adapted tissue Doppler imaging (TDI) (Kanai 2005; Brekke et al. 2014; Strachinaru et al. 2017). Other studies have demonstrated the feasibility of measuring the SWs induced by AVC and MVC in a single recording using diverging waves (Vos et al. 2017; Petrescu et al. 2019; Santos et al. 2019). Slope-estimator, intra-observer, inter-observer and test-retest variabilities have been recently tested for natural SWs in healthy volunteers (Santos et al. 2019). However, we have observed that anatomic M-line location on the IVS, along which the SWs are tracked, affects the measured propagation speed in pigs, causing intra-scan variability (Keijzer et al. 2018). Furthermore, other than test-retest variabilities between measurements performed on different days, variabilities between subsequently performed measurements could have been present. In addition, Santos et al. (2019) performed SWS measurements with only one (non-clinical) echographic scanning system, but inter-system variability should be limited for clinical diagnosis. Also, hemodynamic variations could have caused variabilities in SWS measurements. When patients undergo an echocardiographic exam, they may experience various levels of psychologic and/or physiologic stress, potentially changing loading conditions and thus affecting SWS measurements.

To the best of our knowledge, our study is the first to simultaneously report on inter-system, test-retest, inter-scan, intra-scan and inter-observer variabilities of natural SWS measurements after AVC and MVC in healthy volunteers and to report on the effect of stress causing hemodynamic variations. To test inter-system variability, we directly compared the results obtained by

Table 1. Overview of the demographic characteristics of the study population*

Characteristic	Mean ± standard deviation	Range
Age (y)	29.8 ± 6.2	24–45
Weight (kg)	67 ± 9.5	55–90
Body length (m)	1.75 ± 0.06	1.65–1.83
Body Mass Index (weight/body length^2 [kg/m^2])	21.9 ± 2.3	19.4–27.5
Heartrate in rest (bpm)	62 ± 7	50–73
Systolic blood pressure in rest (mm Hg)	106 ± 13	90–138
Diastolic blood pressure in rest (mm Hg)	62 ± 9	50–81
Heartrate during handgrip test (bpm)	67 ± 8	51–81
Systolic blood pressure during handgrip test (mm Hg)	110 ± 10	94–138
Diastolic blood pressure during handgrip test (mm Hg)	67 ± 9	52–85

* The characteristics are averaged over all volunteers during both scanning sessions.

using a clinical system in a conventional TDI mode (Philips) with a second clinical system with a customized high frame rate (HFR) mode, using a diverging-wave pulse-inversion transmission scheme (Zonare).

MATERIALS AND METHODS

Study population

The study included 10 volunteers aged 24–45 y, 5 males and 5 females. Table 1 presents an overview of the demographic characteristics of the volunteers. The study was approved by the local medical ethics committee (Erasmus MC MEC-2014-611) and all volunteers provided informed consent. The following exclusion criteria were used: a history of cardiovascular disease, cardiovascular risk factors including hypertension (cut-off value of 140/90 mm Hg), being pregnant or being morbidly obese (body mass index > 40 kg/m^2).

Data acquisition

An overview of the study design and the tested variabilities are presented in Figure 1. Measurements were performed with 2 echographic scanning systems. First, a clinical system programmed by the manufacturer to have a HFR imaging mode (Zonare ZS3, P4-1 C probe, Mindray Innovation Center, San Jose, CA, USA) was used. Live B-mode images with a low frame rate (LFR) were used to position the probe. Then a smaller box (approximately 5 × 7 cm) was selected within these LFR images for the HFR acquisition. During these recordings, the LFR images were frozen on the screen of the system and no live feedback was present. A diverging-wave pulse-inversion transmission sequence was used for the HFR acquisition, and beamformed in-phase and quadrature components (IQ-based data) with a frame rate of 1000 frames/second during 1.2 s were saved for offline processing. In this way, at least a full cardiac cycle was measured for a minimum heartrate of 50 bpm. The acquisitions with this machine were carried out by a sonographer (D.J.B.). Second, acquisitions were performed by a cardiologist (M.S.) with a clinical echographic scanner in conventional TDI mode (Philips iE33, S5-1 probe, Philips, Bothell, WA, USA). To obtain maximum frame rates, a balance between opening angle and depth of TDI field was searched for, as described by Strachinaru et al. (2017). In this way frame rates from 490–570 frames/second were realized. Simultaneously a phonocardiogram (PCG) (Fukuda Denshi MA-300 HDS (V), Fukuda Denshi Co., Tokyo, Japan) was recorded, and the electrocardiographic signal was used as a trigger.

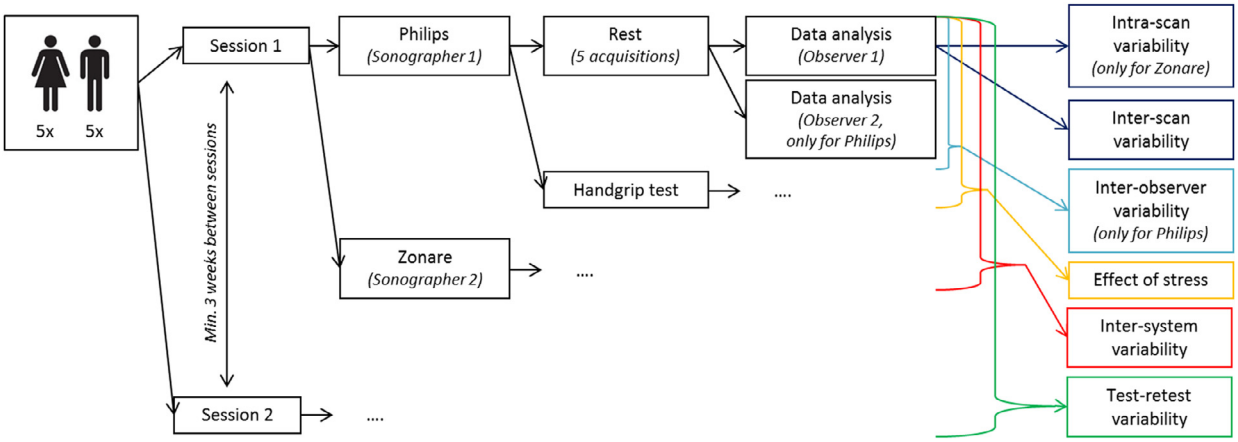

Fig. 1. Schematic overview of the study design. The same measurements were performed during session 1 and session 2. Rest and handgrip test measurements were performed with the Zonare and the Philips system. Inter-observer variability was tested for the Philips system only, and intra-scan variability was only tested for the Zonare system.

All data during 2 cardiac cycles were saved in Digital Imaging and Communications in Medicine (DICOM) format for offline processing.

For every volunteer, first 5 long-axis parasternal view measurements, with intermittent probe repositioning, were performed with the Zonare system. It was ascertained that both aortic and mitral valves were in the image plane. Directly after the measurements with the Zonare system, measurements were repeated with the Philips system. Subsequently, the effect of physiologic stress causing hemodynamic variations on the SWS measurements was tested by performing handgrip tests. During the handgrip measurements, the volunteers were asked to keep a stress ball continuously squeezed with their left hand. While volunteers kept on squeezing, measurements were repeated with both machines. All measurements were performed within 30 min per volunteer. Furthermore, to investigate test-retest variability, all measurements were repeated per volunteer during a second scanning session on a separate day. The time period between the first and second session for the volunteers varied between 21 and 93 d.

Shear wave propagation speed analysis

The propagation speeds of the SWs induced by the AVC and MVC were determined by using different methods for the Zonare and Philips system. Although one method applicable to the data of both systems could be searched for, we choose to use different methods that were more suitable for the data format of the individual systems.

Clinical system with custom HFR mode. Offline IQ-based data stored from the Zonare system were analyzed in Matlab R2017a (MathWorks, Natick, MA, USA). To remove high frequency TDI information that was for the most part corresponding to blood and noise, a sixth order lowpass Butterworth filter with a cut-off frequency of 250 Hz was applied to the IQ data in slowtime. Axial tissue velocities were obtained by using a one-lag autocorrelation technique (Brekke et al. 2014). To reduce the effect of speckle and noise, a Gaussian spatial smoothing filter with a size of 4 mm by 6.7° was applied to the autocorrelation frames before calculating the phase (Brekke et al. 2014; Strachinaru et al. 2017; Vos et al. 2017). The moments of AVC and MVC were visible in the B-mode images. However, because the HFR box was relatively small, the aortic valves were not visible in all recordings; but, they were visible in the LFR overview images captured in the seconds before and after the HFR recordings. Therefore, the moments of valve closure in the HFR acquisitions were determined based on the movement of the mitral valves, on the overall motion of the heart and on the derived TDI movies. For each recording, an anatomic M-line was manually drawn on the basal-mid part of the IVS at the moment of valve closure (Fig. 2a, 2d). Depending on the position of the IVS in the field of view and on the visible propagation length of the SWs,

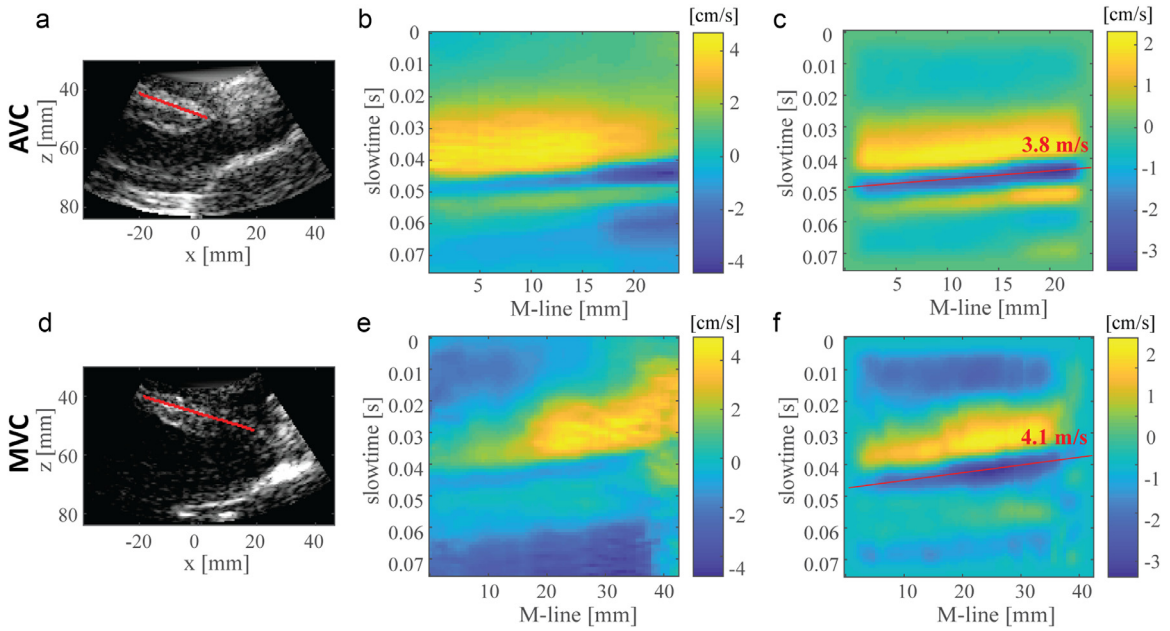

Fig. 2. Zonare: Example of an M-line drawn at (a) AVC and (d) MVC. The corresponding M-panels are presented in (b) and (e), respectively. After applying a BPF, we applied a Radon transform to obtain the propagation velocities as presented in (c) and (f).

the length of the M-line varied between 1.9−4.1 cm (AVC) and 2.1−5.7 cm (MVC). Then, the axial particle velocities over the M-line were assembled in a motion-panel (M-panel) for a period of 75 ms around the moment of valve closure. The SWs induced by the AVC and MVC are depicted as wave patterns propagating over slowtime along the M-lines in the M-panels (Fig. 2b, 2e). The slope of these patterns represents the propagation speed of these SWs. The AVC and MVC occur during the isovolumetric relaxation and isovolumetric contraction phase, respectively, and therefore no gross motion was assumed nor seen to be present. Nonetheless, a sixth order bandpass Butterworth filter between 15 and 100 Hz was applied to the axial tissue velocities in slowtime, because the SWs were observed to be in this frequency range. Therefore, also any offset attributable to gross motion was removed. To obtain the propagation speeds of the SWs induced by the various valve closures, the slope of the patterns presented in the M-panels was determined by using a Radon transform (Rouze et al. 2010; Song et al. 2013; Vos et al. 2017)(Fig. 2c, 2f). Before applying the Radon transform, the M-panels were first resampled to have an equal number of pixels in space and time and then tapered in both directions. Furthermore, the Radon domain was normalized, as described by Vos et al. (2017). The minimum intensity, corresponding to the particle motion away from the transducer, was selected in the Radon domain to determine the propagation speed. As also reported in data regarding pigs (Keijzer et al. 2018), the location of the manually drawn M-line was observed to affect the results. Therefore, to test intra-scan variability for every recording, the M-lines were drawn 10 times. The location of these M-lines was chosen based on the visibility of the SW propagation. When the SW propagation was observed to be less reliable on the right and left ventricle sides of the IVS, M-lines were drawn more to the middle. Analysis of the Zonare data was done by the researcher who wrote the MATLAB analysis script (L.B.H.K.). Other than determining the moments of valves closure and drawing the M-lines, the data analysis process was fully automated. Because 10 M-lines were already drawn for every recording, inter-observer variability testing was not considered meaningful for the Zonare system.

For every volunteer 7 measurements were performed per session, leading to 140 measurements in total. SWs after AVC and MVC were tracked in 122/140 (87%) and 92/140 (66%) measurements, respectively. The main reasons to exclude recordings from the measurements were a poor B-mode quality (approximately 5% of measurements after AVC and/or MVC), or the IVS moving out of the field of view (approximately 5%). Furthermore, acquisitions with no visible propagating SWs or with propagation over only short distances (<1.8 cm [approximately 20%]) were excluded. For 1 volunteer (volunteer 8), propagating SWs after MVC could not be seen in any recording.

Clinical system with clinical HFR mode. The Philips QLab8 software program (Bothell, WA, USA) was used for post-processing of the Philips DICOM data as described elsewhere (Strachinaru et al. 2017). The method is repeated here in brief. Because the depth and width of the TDI was minimized to obtain high frame rates, valves were not visible in the measurements. Therefore, the moments of valve closure were determined based on the PCG signals (onset of the heartsounds (S), S1 and S2) and the appearance of SWs in TDI (Fig. 3). Although the moment of valve closure could not visually be determined

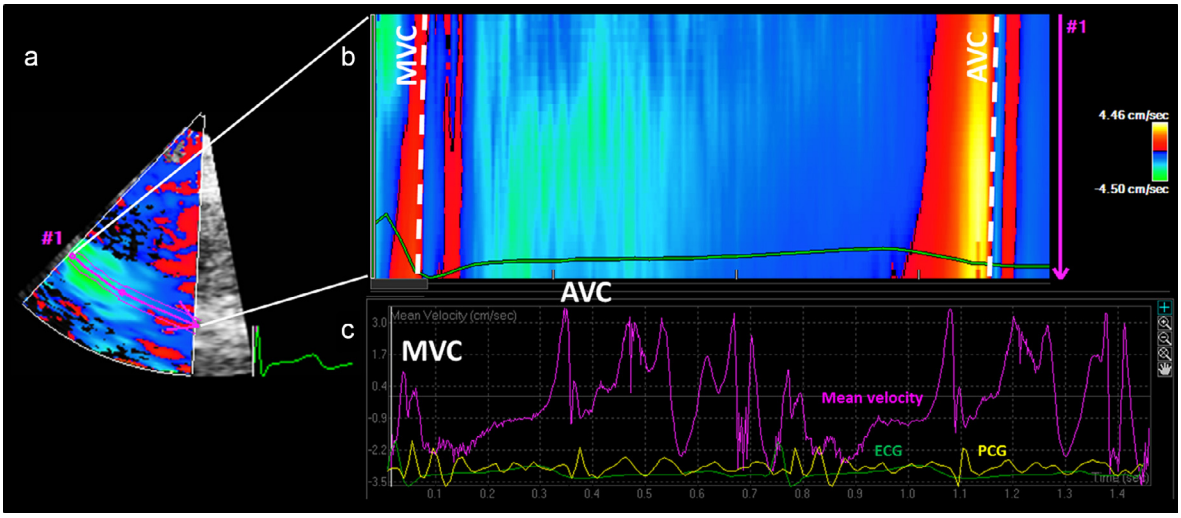

Fig. 3. Philips: Example of a measurement where SWs were tracked after AVC and MVC. The Philips QLab8 software program shows (a) the TDI movie, (b) the M-panel and (c) the mean velocity curve.

in the B-mode images, the onset of heart sounds are well known to correspond to valve closure. Furthermore, natural SWs induced by valve closure propagate from the aortic root to the apex (Vos et al. 2017; Strachinaru et al. 2019), unlike electromechanical waves starting at midlevel of the IVS and propagating toward base and apex (Provost et al. 2011). Anatomic M-lines were manually drawn over the IVS, and the length of these M-lines was defined based on the width of the TDI field of view. This length ranged between 2 and 3 cm. Subsequently, an M-panel and a mean tissue velocity curve were provided by the software (Fig. 3). By viewing the pattern shown on the M-panel (b), the tissue velocity curve (c) and the TDI movie (a) itself, the period needed for the SW to propagate over the M-line was determined. Because data analysis was not automated and the TDI data of the entire septum could be used as a reference by viewing the TDI movies, the effect of M-line location was minimal. Therefore, only 1 M-line was drawn per recording. The transition from positive to negative TDI values of the SWs were tracked, because these were most visible to the observer. Because the SWs were tracked visually, inter-observer variability was considered as an important factor. Analysis of the Philips data was done by the same researcher who analyzed the Zonare data (L.B.H.K). To test inter-observer variability, data analysis of the Philips measurements was repeated by a cardiologist experienced with the post-processing software (M.S.), blinded to earlier values.

For the Philips system, SWs could be tracked after AVC in 365/474 (77%) and after MVC in 71/474 (15%) recorded cardiac cycles. In this study we measured the SWs after AVC and MVC in single recordings. TDI limits were chosen for the visualization of the SWs after AVC, because these had our focus for the measurements. Lower TDI limits might have been chosen when focusing on the SWs induced by MVC, because these have lower magnitudes. Therefore, the transition from positive to negative TDI values after MVC was not visible in many DICOM images, and we obtained a low feasibility for the MVC measurements compared with the MVC data with this method (Strachinaru et al. 2019). Furthermore, values above 10 m/s were removed because they were assumed to be non-physical, as was done by Vos et al. (2017).

Statistics

Statistical analysis was done by using a statistical toolbox in MATLAB R2017a (Natick, MA, USA). Kolmogorov-Smirnov tests were used to test for normal distributions. Propagation speeds are presented as median values and interquartile ranges (IQR). To compare our results with literature values, mean and standard deviations were also reported. We observed that some volunteers were nervous when entering the scanning room. To test whether all measurements in rest could be grouped, the first and last of five rest measurements were compared. A Wilcoxon signed-rank test was applied to the median values per recording for the Zonare data and to the individual values per heart cycle for the Philips data. Also, a Bland-Altman analysis was used to depict differences (mean differences, limits of agreement [LOA] and range). A similar analysis was done to test the effect of the handgrip test and the test-retest and inter-system variability. For the Zonare data, intra-scan variability was investigated by computing the median of all IQRs of the values obtained per measurement for the 10 M-lines of all rest and stress measurements. The median value of the IQRs of the median recording values was used to measure inter-scan variability.

RESULTS

Hemodynamic characteristics

Average blood pressures of 106 ± 13 mm Hg (systolic) and 62 ± 9 mm Hg (diastolic) were measured in rest, and average pressures of 110 ± 10 mm Hg and 67 ± 9 mm Hg were measured during the handgrip test. The diastolic blood pressure was statistically significantly different during the handgrip test ($p = 0.0088$) but the systolic blood pressure was not ($p = 0.077$). Also the heart rate, measured with the electrocardiogram (ECG) connected to the Philips system, was observed to increase significantly ($p < 0.01$) from 62 ± 7 bpm to 67 ± 8 bpm.

Clinical system with custom HFR mode

Figure 4 presents the results obtained for the 10 volunteers for the AVC and MVC, respectively. The median values in rest ranged from 3.23−4.25 m/s for AVC and from 2.06−4.72 m/s for MVC. These median values were not normally distributed. Furthermore, we cannot assume that all volunteers have the same SW propagation speeds. Nevertheless, for comparison with other studies, the mean and standard deviations of these median values were computed to be 3.8 ± 0.4 m/s (AVC) and 3.4 ± 1.0 m/s (MVC). Table 2 presents an overview of the statistical characteristics of all measurements. For every measurement, 10 M-lines were drawn over the IVS. The IQRs per measurement presented in Figure 4 thus represent the intra-scan variabilities. For the AVC measurements in rest, a median value of 0.38 m/s (IQR: 0.26−0.68 m/s) was observed for all IQRs, for the MVC measurements in rest this was observed to be 0.26 m/s (IQR: 0.15−0.46 m/s). The variations in median values per recording per volunteer were used as measure for the inter-scan variability. The median IQRs of median values in rest per volunteer per session were observed to be 0.67 m/s (IQR: 0.40−0.86

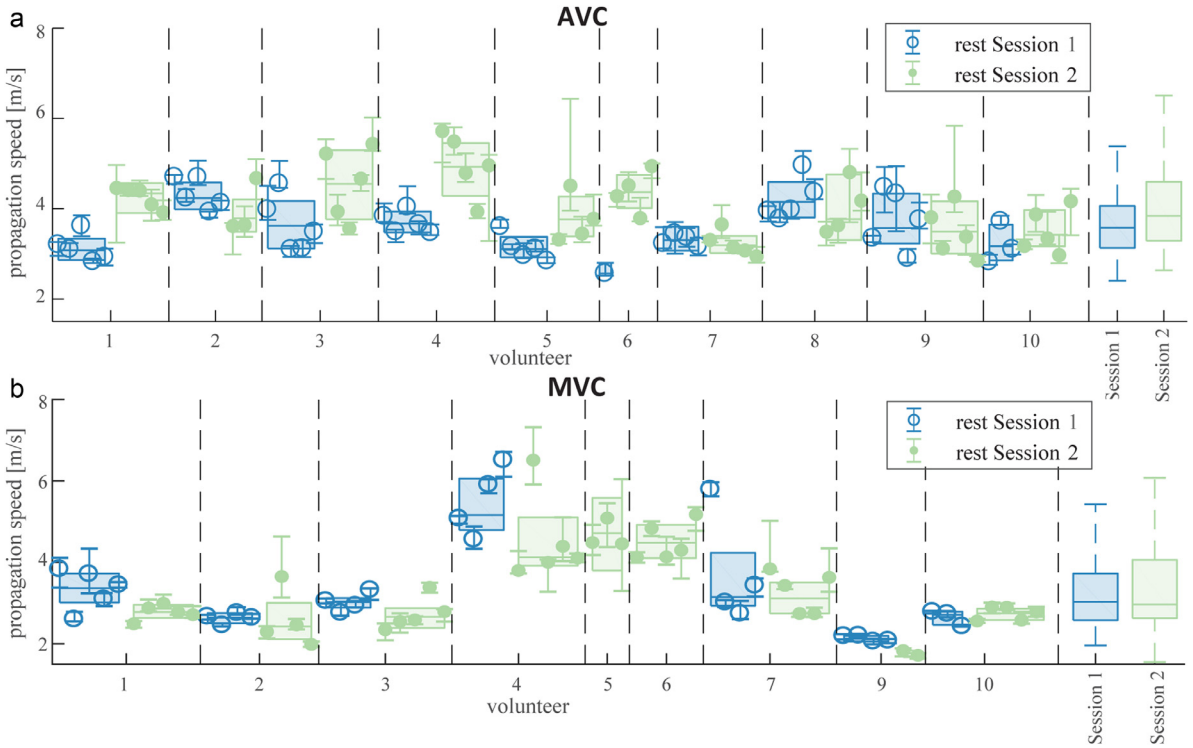

Fig. 4. Zonare: Median values and IQRs of the measurements in rest performed for (a) the AVC and (b) the MVC. For every recording, 10 M-lines were drawn over the IVS. The IQRs depict the intra-scan variabilities. Inter-scan variabilities (median values and IQRs) per volunteer for every session are depicted in boxplots. Inter-scan variabilities were observed to be slightly higher than, but in similar ranges as, intra-scan variabilities.

m/s) for the AVC and 0.61 m/s (IQR: 0.26−0.94 m/s) for the MVC. To test whether all rest measurements could be grouped despite a possible time-dependency during the period of the exam, the medians obtained for the first and last rest measurement per volunteer for both sessions were compared (Supplementary Fig. 1a, 1d). Average differences of −0.0017 m/s (LOA: −1.22 to 1.03 m/s) (AVC) and −0.10 m/s (LOA: −1.85 to 1.64 m/s) (MVC) were observed with a Bland-Altman analysis. No statistically significant differences were observed ($p = 0.90$ for AVC and $p = 0.53$ for MVC). Therefore, we grouped all rest measurement per volunteer per session to compute the test-retest variability (Fig. 5). Mean differences of −0.51 m/s (LOA: −2.05 to 1.02 m/s) (AVC) and 0.37 m/s (LOA: −0.35 to 1.08 m/s) (MVC) were observed for the test-retest variability of all measurements, (Supplementary Fig. 1b, 1e). These differences were observed to be just significant for the MVC ($p = 0.047$) but not for the AVC ($p = 0.13$). We grouped both sessions before computing the inter-volunteer variability. The median values of the rest measurements per volunteer were observed to be in the ranges of 3.23−4.25 m/s and 2.06−4.72 m/s for the AVC and MVC, respectively. Subsequently, rest and handgrip measurements are compared (Supplementary Fig. 1c, 1f). Average differences of −0.33 m/s (LOA: −1.94 to 1.27 m/s) for the AVC measurements and −0.072 m/s (LOA: −1.82 to 1.68 m/s) for the MVC measurements were observed. These differences were not observed to be significant ($p = 0.073$ for AVC and $p = 0.56$ for MVC) (Fig. 5).

Clinical system with clinical HFR mode

The propagation speeds obtained from the Philips data are presented in Figure 6. Because the feasibility of the MVC measurements was low, no statistical tests were performed on these few MVC measurements. Therefore only the statistics of the AVC measurements are described here. The median values in rest ranged from 1.82−4.76 m/s (Table 2). As done for the Zonare, mean and standard deviation was computed for illustrative purposes (3.2 ± 0.9 m/s). A median value of the IQRs of the propagation speed values in rest per session per volunteer of 0.71 m/s (IQR: 0.33−1.07 m/s) was observed, representing the inter-scan variability. It should be noted that these values seem to be higher than the inter-scan variability values of the Zonare data, where first median values over the 10 M-lines per scan were obtained before computing inter-scan variability. As for the Zonare data, no statistically significant difference was observed between the first and last rest measurement

Table 2. Overview of the statistical characteristics of the Zonare and Philips data

Type of variability	Performed test	Zonare		Philips
		AVC	MVC	AVC
Intra-scan	Median of all IQRs of the values obtained per measurement for the 10 M-lines	0.38 m/s, $n = 136$ (IQR: 0.26−0.68 m/s)	0.26 m/s, $n = 99$ (IQR: 0.15−0.46 m/s)	-
Inter-scan	Wilcoxon signed-rank test on medians of first and last rest measurement per volunteer per session	$p = 0.90$, $n = 19$	$p = 0.53$, $n = 16$	$p = 0.15$, $n = 20$
	Bland-Altman: medians of first − medians of last rest measurement per volunteer per session	Mean: −0.0017 m/s, $n = 19$ (LOA: −1.22 to 1.23 m/s) (Range: −1.06 to 0.96 m/s)	Mean: −0.10 m/s, $n = 16$ (LOA: −1.85 to 1.64 m/s) (Range: −1.56 to 2.36 m/s)	Mean: −0.36 m/s, $n = 20$ (LOA: −2.29 to 1.58 m/s) (Range: −2.63 to 1.06 m/s)
Inter-scan	Median of all IQRs of (median) rest values per volunteer per session	0.67 m/s, $n = 19$ (IQR: 0.40−0.86 m/s)	0.61 m/s, $n = 16$, (IQR: 0.26−0.94 m/s)	0.71 m/s, $n = 19$ (IQR: 0.33−1.07 m/s)
Test-retest	Wilcoxon signed-rank test on medians of all rest measurements per volunteer for Session 1 and Session 2	$p = 0.13$, $n = 10$	$p = 0.047$,* $n = 7$	$p = 0.28$, $n = 10$
	Bland-Altman: medians of all rest measurements per volunteer for session 1- for session 2	Mean: −0.51 m/s, $n = 10$ (LOA: −2.05 to 1.02 m/s) (Range: −1.81 to 0.45 m/s)	Mean: 0.37 m/s, $n = 7$ (LOA: −0.35 to 1.08 m/s) (Range: −0.034 to 1.04 m/s)	Mean: −0.19 m/s, $n = 10$ (LOA: −1.59 to 1.21 m/s) (Range: −1.44 to 1.19 m/s)
Inter-volunteer	Range of median rest values per volunteer	3.23−4.25 m/s, $n = 10$	2.06−4.72 m/s, $n = 9$	1.82−4.76 m/s, $n = 10$
Handgrip test	Wilcoxon signed-rank test on medians of all rest and all handgrip test measurements per volunteer per session	$p = 0.073$, $n = 20$	$p = 0.56$, $n = 15$	$p = 0.079$, $n = 19$
	Bland-Altman: medians of all rest − medians of all handgrip test measurements per volunteer per session	Mean: −0.33 m/s, $n = 20$ (LOA: −1.94 to 1.27 m/s) (Range: −3.07 to 0.74 m/s)	Mean: −0.0723 m/s, $n = 15$ (LOA: −-1.82 to 1.68 m/s) (Range: −2.22 to 0.93 m/s)	Mean: −0.39 m/s, $n = 19$ (LOA: −2.22 to 1.44 m/s) (Range: −2.38 to 1.49 m/s)
Inter-observer	Wilcoxon signed-rank test on medians of rest measurement per volunteer per session analyzed by observer 1 and observer 2	-	-	$p = 0.35$, $n = 20$
	Bland-Altman: medians of all rest measurements per volunteer per session for observer 1 − for observer 2	-	-	Mean: 0.11 m/s, $n = 20$ (LOA: −1.42 to 1.65 m/s) (Range: −1.55 to 1.21 m/s)
				AVC
Inter-system	Wilcoxon signed-rank test on median rest values per volunteer per echographic scanner			$p = 0.044$,* $n = 20$
	Bland-Altman on median rest values per volunteer per echographic scanner bias + limits of agreement			Mean −0.43 m/s, $n = 20$ (LOA: −2.23 to 1.37 m/s) (Range: −1.95 to 1.08 m/s)
				Zonare
AVC versus MVC	Median ratio of median rest values per volunteer per session for AVC and MVC			1.20, $n = 16$ (IQR: 1.00−1.58)
	Median difference of median rest values per volunteer per session for AVC and MVC			0.64 m/s, $n = 16$ (IQR: −0.019 to 1.50 m/s)

* The p -value corresponds to a statistically significant difference ($p < 0.05$).LOA = limits of agreement Bland-Altman analysis (±1.96 SD).

per volunteer per session ($p = 0.15$). A Bland-Altman analysis showed a mean difference between the first and last rest measurement of −0.36 m/s (LOA: −2.29 to 1.58 m/s) (Supplementary Fig. 2a). Therefore, all rest measurements were grouped for measuring the test-retest variability. A mean difference of −0.19 m/s (LOA of −1.59 to 1.21 m/s) was observed, which was not statistically significant ($p = 0.28$) (Supplementary Fig. 2b). Therefore, as for the Zonare data, the measurements in session 1 and session 2 were grouped to obtain inter-volunteer variability ranges. The median rest values per volunteer were observed to be in the range of 1.82−4.76 m/s. Also similar to the Zonare data, the difference between rest and stress measurements was not observed to be significant ($p = 0.079$). A mean

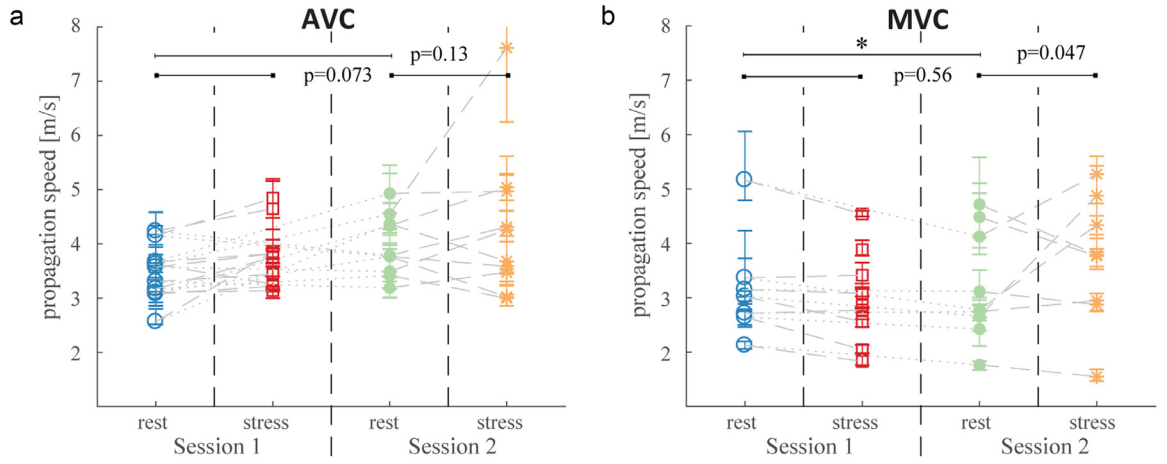

Fig. 5. Zonare: Comparison of the median values and IQRs of the rest and stress measurements of session 1 and session 2 per volunteer for (a) AVC and (b) MVC. Test-retest differences were observed to be just significant for the MVC, but not for the AVC. No significant effect was observed for the handgrip test (rest vs. stress).

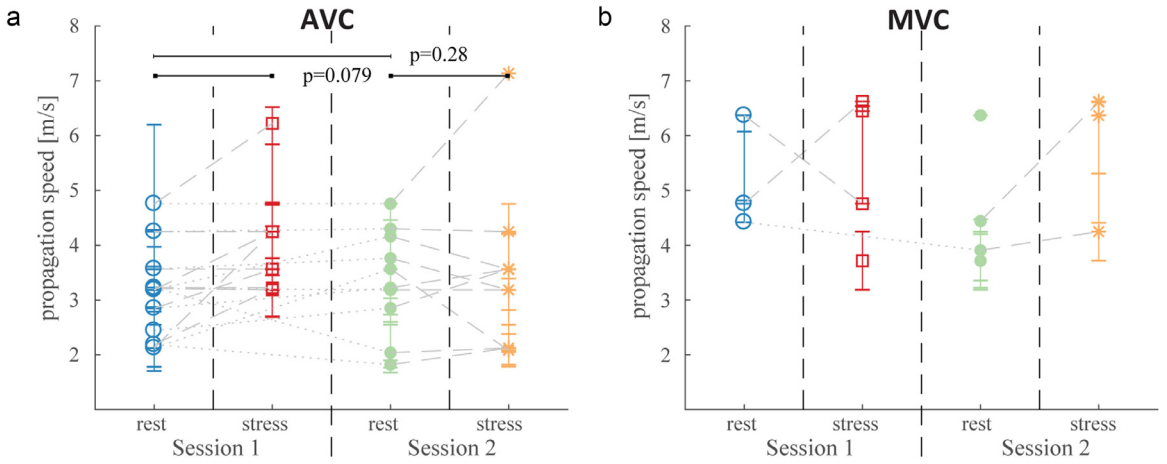

Fig. 6. Philips: Comparison of the median values and IQRs of the rest and stress measurements of session 1 and session 2 per volunteer for (a) AVC and (b) MVC. No statistical tests were performed on the MVC measurements because of a low feasibility. For the AVC measurements, no significant effects were observed for test-retest and the handgrip test.

difference of −0.39 m/s (LOA: −2.22 to 1.44 m/s) was observed.

Intra-scan variability was not tested for the Philips data, because only 1 M-line curve and thus 1 propagation speed value was obtained per heart cycle with the Philips system. Instead of intra-scan variability, inter-observer variability was measured for the Philips data. The second observer computed propagation speeds per volunteer per session averaged over 3 heart cycles. These propagation speeds were compared with the median rest values obtained by the first observer. An average difference of 0.11 m/s (LOA: −1.42 to 1.65 m/s) was observed (Supplementary Fig. 3), which was not observed to be significant ($p = 0.35$). The feasibility of the MVC measurements was higher for the second than for the first observer. Although the first observer obtained propagation speeds in 7 sessions, the second observer obtained values for 14 sessions. Nonetheless, for consistency, no statistical tests were performed on the MVC measurements analyzed by the second observer.

Comparison of the systems

Because of the the low feasibility of the MVC measurements with the current settings on the Philips system, only the AVC measurements of the Zonare and the Philips system were compared. The difference in results obtained with the Zonare and the Philips system was observed to be statistically significant ($p = 0.044$). The Bland-Altman analysis shows a median bias of −0.43 m/s (LOA: −2.23 to 1.37 m/s), indicating that we consistently measured a lower propagation speed with the Philips system (Supplementary Fig. 4).

As suggested by others (Vos et al. 2017; Santos et al. 2019), the difference and ratio of the propagation speeds obtained for the AVC and MVC might be of clinical relevance because of hemodynamics. Because of the low feasibility of the MVC measurements with the Philips system, these ratios and differences were only computed for the Zonare system (Supplementary Fig. 5). The median ratio and difference were observed to be 1.20 (IQR: 1.00 to 1.58) and 0.64 m/s (IQR: −0.019 to 1.50 m/s), respectively.

DISCUSSION

In this study, we tested the reproducibility of the propagation speeds of natural SWs induced by the AVC and the MVC in 10 healthy volunteers. For the AVC measurements, no statistically different propagation speeds were obtained on different days. Our results suggest that the variabilities of natural SWS measurements are dominated by measurement inaccuracies rather than mild hemodynamic variations. Statistically, different propagation speeds after AVC were obtained for two different systems.

Measurement variations can have physiologic causes or can arise because of measurement inaccuracies. Intra-scan variability is measured within individual recordings, and, therefore, physiologic causes are assumed to be non-existing. Inter-scan variabilities can also occur because of physiologic variations, and these variations are expected to be even larger when comparing different sessions. We observed inter-scan variabilities (Zonare: 0.67 m/s [IQR: 0.40−0.86 m/s] for AVC and 0.61 m/s [IQR: 0.26−0.94 m/s] for MVC) to be slightly higher than, but in similar ranges as, intra-scan variabilities (Zonare: 0.38 m/s [IQR: 0.26−0.68 m/s] for AVC and 0.26 m/s [IQR: 0.15−0.46 m/s] for MVC). Moreover, test-retest variabilities were observed to also be in similar ranges as inter-scan variabilities (Supplementary Figs. 1 and 2). Therefore, our results suggest that the measurement variations were dominated by several measurement inaccuracies, which are expected to have different causes. First, we observed qualitatively that contrast in the B-mode images affected the results. For recordings with a low visible contrast between tissue and blood, we experienced that positioning the M-lines on the IVS was more challenging. This was especially important for the Zonare system, where a diverging-wave transmission scheme was used, and therefore B-mode contrast was sometimes limited because of clutter. Furthermore, clutter could have affected the determination of tissue velocities. Second, the SWs could only be tracked over the limited visible length of approximately 3 cm of the IVS. An SW with a center frequency of, for example 50 Hz (Santos et al. 2019) and a propagation speed of 3.5 m/s, has a wavelength of 7.0 cm. This means that only a fraction of this wavelength can be tracked, which causes measurement inaccuracy, increasing with propagation speed.

In a uniform shear wave phantom with ARF-push−induced shear waves, Strachinaru et al. (2017a) obtained similar propagation speeds with a research scanner as with the clinical Philips system. However, for the AVC measurements, we obtained statistically different propagation speeds with the Philips system compared with the Zonare system. As the measurements with the different systems were performed within half an hour per session, the differences are expected to be mainly attributable to the differences in data processing for the different systems. First, for the Zonare measurements, a Radon transform was used to track the maximum negative particle velocities, but for the Philips measurements, the onset of the wave, as visible from positive to negative tissue velocities, was tracked. This means that slightly different aspects of the SW pattern were tracked. We have observed in measurements in an animal model different propagation speeds as well when tracking different rims of the SWs (Keijzer et al. 2018). Second, although a frame rate of 1000 Hz was used for the Zonare, frame rates varied between 490 and 570 Hz for the Philips system, and therefore the time resolution differed by a factor of 2. This is expected to induce more uncertainties and thus more variability (Strachinaru et al. 2017), as observed in our study (Figs. 5 and 6). Third, the SWs were tracked automatically with the Radon transform for the Zonare system, and, for the Philips system, visual feedback obtained from the M-panel, the tissue velocity curve and the TDI movie was used to determine the propagation speeds. Therefore, when comparing different studies, these methodologic aspects should also be taken into account. Furthermore, the effect of using different systems and methods should be studied also for pathologic hearts in more detail.

The advantage of using the Radon transform for the Zonare system is that data analysis can be more automated. To minimize the effect of noise, we applied a lowpass filter to the IQ data in slowtime. Furthermore, a Gaussian spatial smoothing filter was applied to the autocorrelation frames. In addition, for every measurement 10 M-lines were drawn over the IVS. Moreover, we interpolated the M-panels to a panel with an equal number of pixels in space and time. We also normalized the Radon domain by dividing by the Radon transform of a panel with an equal number of pixels with only unit values, to avoid an apparent bias (Vos et al. 2017). To further reduce the effect of noise, the performance of using a least-squares or high resolution Radon transform (Thorson and Claerbout 1985) could be investigated in the future.

The potential hemodynamic variation attributable to psychologic stress related to the examination was estimated by comparing the first and last rest measurement within a session. No significant differences were observed. This indicates that, when patients are nervous at the beginning of a scanning session, this does not strongly affect these measurements, which is beneficial for the application of clinical diagnosis. Nonetheless, it should be noted that the number of measurements in this study was limited and thus not enough statistical power may be present to detect small differences. Therefore, to investigate the effect of larger variations in hemodynamics, a handgrip test was performed during the SWS measurements. This test is not only relevant for the different levels of physiologic stress patients may experience, but also because diastolic dysfunction patients might show normal hemodynamic characteristics in rest, but have abnormal LV diastolic pressures during exercise (Nagueh et al. 2016). Although heart rate did increase significantly during the handgrip test, the propagation speeds obtained during rest and the handgrip test were not observed to be statistically different. It should be noted that for AVC we observed p values only slightly above $p = 0.05$ ($p = 0.073$ and $p = 0.079$ for Zonare and Philips, respectively). Possibly, the statistical power could be too limited to measure significant differences. For the AVC, we did find a mean increase in propagation speed during stress of 0.33 m/s and 0.39 m/s with the Zonare and Philips system, respectively (Supplementary Figs. 1 and 2). Nonetheless, the differences between the measurements in rest and during the handgrip test are in the same range as the inter-scan variabilities (Supplementary Figs. 1 and 2). This suggests that no extra variabilities are induced because of the handgrip test. However, only low levels of stress causing small hemodynamic changes are induced by handgrip tests. Although higher levels of stress could be induced by using an exercise test, performing HFR acquisitions would be more challenging. Whether the measurement of the natural SWs induced by AVC and MVC is completely independent of loading conditions should be further investigated in a study with higher statistical power.

Several studies have reported on the propagation speed of SWs in healthy volunteers, as summarized in Table 3. Some studies used a long-axis parasternal view, but Brekke et al. (2014) used a 4-chamber apical view. However, the exact effect of the imaging view on the measured propagation speed is currently unclear. The propagation speeds obtained in this study for the SWs after AVC are in the same range as the values measured in other human studies. Some studies used ARF to induce SWs during diastole in healthy volunteers. However, these values cannot be directly compared with the values obtained after closure of the valves, because the timing of the measurements is different. MVC and AVC occur around the onset of contraction and relaxation, respectively (Remme et al. 2008). Other studies have shown stiffness variation over the cardiac cycle in animals (Couade et al. 2011; Pernot et al. 2011; Vejdani-jahromi et al. 2015) and human (Tzschätzsch et al. 2012; Hollender et al. 2017). Couade et al. (2011) reported on an increase in shear modulus from approximately 5 kPa to 15 kPa in the first 50 ms after the R peak in sheep,

Table 3. Overview of human shear wave elastography measurements described in the literature

Natural SWS				
Study	View	Subject	MVC	AVC
Kanai (2005)	PLAX, IVS	Healthy volunteer	-	1−7 m/s (10−90 Hz)
Brekke et al. (2014)	AP4 C, IVS	Healthy volunteers	-	5.41 ± 1.28 m/s
Santos et al. (2019)	PLAX, IVS	Healthy volunteers	3.2 ± 0.6 m/s (2.1−4.4 m/s)	3.5 ± 0.6 m/s (2.2−4.5 m/s)
Petrescu et al. (2019)	PLAX, IVS	Healthy volunteers	3.54 ± 0.93 m/s	3.75 ± 0.76 m/s
		Cardiac amyloidosis	6.33 ± 1.63 m/s	5.63 ± 1/13 m/s
Strachinaru et al. (2019)	PLAX, IVS	Healthy volunteers	4.65 ± 0.77 m/s (3.25−6.50 m/s)	3.61 ± 0.46 m/s (3.10−4.66 m/s)
		HCM patients	6.88 ± 1.22 m/s (5.45−8.91 m/s)	5.13 ± 0.68 m/s (3.75−6.94 m/s)
Keijzer et al. (present study)	PLAX, IVS	Healthy volunteers	Zonare 3.4 ± 1.0 m/s (2.06−4.72 m/s)	Zonare 3.8 ± 0.4 m/s (3.23−4.25 m/s)
			-	Philips 3.2 ± 0.9 (1.82−4.76 m/s)

ARF based SWS				
Study	View	Subject	End-diastole	End-systole
Song et al. (2016)	LAPV and PSAX, LVFW and IVS	Healthy volunteers	1.29−1.96 m/s	-
Villemain et al. (2019)	PLAX and PSAX, IVS	Healthy volunteers	2.1 ± 1.30* m/s	-
		HCM Patients	3.56 ± 1.71* m/s	-

* Speed values c obtained by converting elasticity values E, using $E = \rho c^2$ with a tissue density ρ of 1000 kg/m^3.HCM = hypertrophic cardiomyopathy, PLAX = parasternal long-axis view, PSAX = parasternal short-axis view, AP4 C = apical 4-chamber view, LVFW = left ventricular free wall, IVS = inter-ventricular septum.

which corresponds to an increase in propagation speed of approximately 70%. With the Zonare system, we observed in general higher values after MVC than ARF-based studies at diastole.

Several authors have suggested that the difference and ratio of the propagation speeds obtained after AVC and MVC are potentially more clinically relevant because of hemodynamics (Vos et al. 2017; Santos et al. 2019). We observed a median difference of 0.60 m/s (IQR: −0.31 to 1.25 m/s) and a mean ratio of 1.21 (IQR: 0.93−1.46) with the Zonare system. However, these values have relatively high variability, likely caused by the combined variability of both the AVC and MVC measurements, which may reduce relevance for clinical diagnosis. Nonetheless, Santos et al. (2019) observed a mean difference of 0.4 ± 0.6 m/s and mean ratio of 1.1 ± 0.2, which is close to the values we obtained. Also, Petrescu et al. (2019) observed higher mean propagation speeds for AVC than for MVC (3.48 ± 0.70 m/s vs. 3.07 ± 0.51 m/s) for healthy volunteers aged 20−39 y. However, for older age groups, no statistical difference was observed between the propagation speeds after AVC and MVC (Petrescu et al. 2019). In contrast, Strachinaru et al. (2019) observed higher propagation speeds for MVC than for AVC (4.68 ± 0.66 m/s vs. 3.51 ± 0.38 m/s) in healthy volunteers. What exact clinically relevant information can be obtained from natural SWS measurements should be further investigated.

Both systems have their own advantages and disadvantages to be used for clinical diagnosis with SWS. The translation of using the clinical Philips system and its clinical data analysis package to daily clinical practice takes less time, which is a major advantage. However, the Zonare system saves IQ data rather than DICOM data, providing the possibility to apply different tracking and filter methods and to automate data analysis. Furthermore, with the Zonare system, a two times higher frame rate is obtained, theoretically corresponding to lower measurement variabilities. The higher feasibility of measuring the SWs after MVC and AVC for the Zonare system is another important advantage. In addition, the inter-volunteer range was observed to be smaller or similar, depending on the observer, for the Zonare compared with the Philips system. However, ECG and PCG could not yet be measured with the Zonare system in HFR mode. This practically means that the moment of valve closure had to be determined visually and that measurements could not be linked to a heartrate, because only one heartbeat was recorded per movie. However, we expect that ECG and PCG could be implemented in the HFR mode of the Zonare system in the future. Image quality was higher with the Philips system, and TDI data were directly shown on the Philips system. This made it easier to perform a more direct quality check of the recording than with the Zonare system. However, when performing the measurements with the Philips system, separate recordings should be made for the AVC and MVC measurements because the TDI velocity scale needs optimization for either measurement. Strachinaru et al. (2019) showed much higher feasibilities for the MVC measurements (89% of 45 healthy volunteers) by using the same system but by performing separate recordings for measuring the SWs after AVC and MVC. For the Zonare system, AVC and MVC measurements can be performed simultaneously. As such, in this stage of developments, both systems can be used as a research bridge to further clinical translation of the technique.

For clinical diagnostic application, it is important to be able to show with a certain amount of confidence significant differences between healthy volunteers and a patient at risk. Our study suggests that measurement variabilities are dominated by measurement inaccuracies. Therefore, by averaging over multiple heartbeats, the standard error is expected to be minimized. The variabilities presented in this study can be used to estimate the minimum amount of measurements needed for clinical diagnosis, once the minimal difference in propagation speed between a patient at risk and a healthy subject are suitably investigated. Considering that data processing is done offline and that measurements can be performed subsequently, we estimate that recording up to 10 heartbeats for averaging is feasible with respect to time and effort.

The ultimate goal is to measure the increased stiffness of the myocardium. However, in this study, we only reported on linear propagation speeds. Because the typical wavelength of the SWs measured (approximately 7 cm) is large compared with the thickness of the IVS (approximately 1 cm), guided waves, rather than bulk shear waves, are expected. Guided waves show dispersion even for purely elastic media, and, thus, measured propagation speeds cannot be directly converted to shear moduli. However, the resolution in the 2-D Fourier domain was restricted because of the limited visible propagation length of the SWs, to measure dispersive effects. Xu et al. (2018) proposed a dispersive Radon transform. However, prior knowledge on the theoretic dispersion curves of the induced modes is needed. Because the IVS is a complex structure with respect to geometry and fiber orientation, we expect that the dispersion curves of Lamb waves in plate structures are too simplistic. As such, the relationship among geometry of the myocardium, propagation speed and early diagnosis of cardiac dysfunction should be further investigated.

CONCLUSIONS

This study investigated the reproducibility of the measurement of propagation speeds of SWs naturally induced by AVC and MVC in healthy volunteers.

Propagation speeds of 3.23−4.25 m/s (AVC) and 2.06−4.72 m/s (MVC) were obtained. Inter-scan variabilities were slightly higher than intra-scan variabilities. For the AVC measurements, no different propagation speeds were obtained after test-retest ($p = 0.13$). However, significantly different values were obtained with a second clinical system (1.82−4.76 m/s for AVC), potentially caused by differences in measurement methods. For this second system, inter-observer variability was tested and no statistical differences were observed. Based on the results of this study, measurement inaccuracies are expected to dominate measurement variations among healthy volunteers. Thus, by averaging over multiple heartbeats, precision for the application of clinical diagnosis can potentially be improved.

Acknowledgments—We thank Dr. G. McLaughlin and Dr. Y. Chen of Mindray Innovation Center (San Jose, CA, USA) for providing the Zonare system with the customized high frame rate imaging mode. This work is part of the STW − Dutch Heart Foundation partnership program "Earlier recognition of cardiovascular diseases" with project number 14740, which is financed (in part) by The Netherlands Organization for Scientific Research (NWO).

Conflict of interest disclosure—The authors declare no competing interests.

SUPPLEMENTARY MATERIALS

Supplementary material associated with this article can be found in the online version at doi:10.1016/j.ultrasmedbio.2019.09.002.

REFERENCES

Arani A, Arunachalam SP, Chang ICY, Baffour F, Rossman PJ, Glaser KJ, Trzasko JD, Mcgee KP, Manduca A, Grogan M, Dispenzieri A, Ehman RL, Araoz PA. Cardiac MR Elastography for quantitative assessment of elevated myocardial stiffness in cardiac amyloidosis. J Magn Reson Imaging 2017a;46:1361–1367.

Arani A, Glaser KL, Arunachalam SP, Rossman PJ, Lake DS, Trzasko JD, Manduca A, McGee KP, Ehman RL, Araoz PA. *In vivo*, high-frequency three-dimensional cardiac MR elastography: Feasibility in normal volunteers. Magn Reson Med 2017b;77:351–360.

Bouchard RR, Hsu SJ, Wolf PD, Trahey GE. *In vivo* cardiac, acoustic-radiation-force-driven, shear wave velocimetry. Ultrason Imaging 2009;31:201–213.

Brekke B, Nilsen LCL, Lund J, Torp H, Bjastad T, Amundsen BH, Stoylen A, Aase SA. Ultra-high frame rate tissue doppler imaging. Ultrasound Med Biol 2014;40:222–231.

Couade M, Pernot M, Messas E, Bel A, Ba M, Hagege A, Fink M, Tanter M. *In vivo* quantitative mapping of myocardial stiffening and transmural anisotropy during the cardiac cycle. IEEE Trans Med Imaging 2011;30:295–305.

Hollender P, Kakkad V, Trahey G. Calibration of ARFI displacements using diastolic shear wave speeds for estimating systolic elasticity. In: IEEE International Ultrasonics Symposium. Piscataway, NJ: IEEE; 2017.

Hollender PJ, Wolf PD, Goswami R, Trahey GE. Intracardiac echocardiography measurement of dynamic myocardial stiffness with shear wave velocimetry. Ultrasound Med Biol 2012;38:1271–1283.

Kanai H. Propagation of spontaneously actuated pulsive vibration in human heart wall and *in vivo* viscoelasticity estimation. IEEE Trans Ultrason Ferroelectr Freq Control 2005;52:1931–1942.

Keijzer LBH, Bosch JG, Verweij MD, de Jong N, Vos HJ. Intra-scan variability of natural shear wave measurements. IEEE International Ultrasonics Symposium. Piscataway, NJ: IEEE; 2018.

Lang RM, Badano LP, Victor MA, Afilalo J, Armstrong A, Ernande L, Flachskampf FA, Foster E, Goldstein SA, Kuznetsova T, Lancellotti P, Muraru D, Picard MH, Retzschel ER, Rudski L, Spencer KT, Tsang W, Voigt JU. Recommendations for cardiac chamber quantification by echocardiography in adults: An update from the American Society of Echocardiography and the European Association of Cardiovascular Imaging. Eur Hear J Cardiovasc Imaging 2015;16:233–371.

Mirsky I, Parmley WW. Assessment of passive elastic stiffness for isolated heart muscle and the intact heart. Circ Res 1973;33:233–243.

Nagueh SF, Smiseth OA, Appleton CP, Byrd BF, Dokainish H, Edvardsen T, Flachskampf FA, Gillebert TC, Klein AL, Lancellotti P, Marino P, Oh JK, Popescu BA, Waggoner AD. Recommendations for the evaluation of left ventricular diastolic function by echocardiography: An update from the American Society of Echocardiography and the European Association of Cardiovascular Imaging. J Am Soc Echocardiogr 2016;29:277–314.

Pernot M, Couade M, Mateo P, Crozatier B, Fischmeister R, Tanter M. Real-time assessment of myocardial contractility using shear wave imaging. J Am Coll Cardiol 2011;58:65–72.

Pernot M, Fujikura K, Fung-Kee-Fung SD, Konofagou EE. ECG-gated, mechanical and electromechanical wave imaging of cardiovascular tissues *in vivo*. Ultrasound Med Biol 2007;33:1075–1085.

Pernot M, Lee WN, Bel A, Mateo P, Couade M, Tanter M, Crozatier B, Messas E. Shear wave imaging of passive diastolic myocardial stiffness: Stunned versus infarcted myocardium. JACC Cardiovasc Imaging 2016;9:1023–1030.

Petrescu A, Santos P, Orlowska M, Pedrosa J, Bézy S, Chakraborty B, Cvijic M, Dobrovie M, Delforge M, D'hooge J, Voigt J-U. Velocities of naturally occurring myocardial shear waves increase with age and in cardiac amyloidosis. JACC Cardiovasc Imaging 2019. doi: 10.1016/j.jcmg.2018.11.029.

Pislaru C, Pellikka PA, Pislaru SV. Wave propagation of myocardial stretch: Correlation with myocardial stiffness. Basic Res Cardiol 2014a;109:438.

Pislaru C, Urban MW, Pislaru SV, Kinnick RR, Greenleaf JF. Viscoelastic properties of normal and infarcted myocardium measured by a multifrequency shear wave method: Comparison with pressure-segment length method. Ultrasound Med Biol 2014b;40:1785–1795.

Ponikowski P, Voors AA, Anker SD, Bueno H, Cleland JGF, Coats AJS, Falk V, González-Juanatey JR, Harjola V-P, Jankowska EA, Jessup M, Linde C, Nihoyannopoulus P, Parissis JT, Pieske B, Riley JP, Rosano GMC, Ruilope LM, Ruschitzka F, Rutten FH, van der Meer P. 2016 ESC guidelines for the diagnosis and treatment of acute and chronic heart failure. Eur Heart J 2016;2129–2200.

Provost J, Lee W-N, Fujikura K, Konofagou EE. Imaging the electromechanical activity of the heart *in vivo*. Proc Natl Acad Sci 2011;108:8565–8570.

Remme EW, Lyseggen E, Helle-Valle T, Opdahl A, Pettersen E, Vartdal T, Ragnarsson A, Ljosland M, Ihlen H, Edvardsen T, Smiseth OA. Mechanisms of preejection and postejection velocity spikes in left ventricular myocardium: Interaction between wall deformation and valve events. Circulation 2008;118:373–380.

Rouze NC, Wang MH, Palmeri ML, Nightingale KR. Robust estimation of time-of-flight shear wave speed using a radon sum transformation. IEEE Trans Ultrason Ferroelectr Freq Control 2010;57:21–24.

Santos P, Petrescu A, Pedrosa J, Orlowska M, Komini V, Voigt J-U, D'hooge J. Natural shear wave imaging in the human heart: Normal values, feasibility and reproducibility. IEEE Trans Ultrason Ferroelectr Freq Control 2019;66:442–452.

Song P, Bi X, Mellema DC, Manduca A, Urban MW, Greenleaf JF, Chen S. Quantitative assessment of left ventricular diastolic stiffness using cardiac shear wave elastography. J Ultrasound Med 2016;35:1419–1427.

Song P, Zhao H, Urban MW, Manduca A, Pislaru SV, Kinnick RR, Pislaru C, Greenleaf JF, Chen S. Improved shear wave motion

detection using pulse-inversion harmonic imaging with a phased array transducer. IEEE Trans Med Imaging 2013;32:2299–2310.
Strachinaru M, Bosch JG, van Dalen BM, van Gils L, van der Steen AFW, de Jong N, Geleijnse ML, Vos HJ. Cardiac shear wave elastography using a clinical ultrasound system. Ultrasound Med Biol 2017;43:1596–1606.
Strachinaru M, Bosch JG, van Gils L, van Dalen BM, Schinkel AFL, van der Steen AFW, de Jong N, Michels M, Vos HJ, Geleijnse ML. Naturally occurring shear waves in healthy volunteers and hypertrophic cardiomyopathy patients. Ultrasound Med Biol 2019;45:1977–1986.
Thorson JR, Claerbout JF. Velocity-stack and slant-stack stochastic inversion. Geophysics 1985;50:2727–2741.
Tzschätzsch H, Elgeti T, Rettig K, Kargel C, Klaua R, Schultz M, Braun J, Sack I. *In vivo* time harmonic elastography of the human heart. Ultrasound Med Biol 2012;38:214–222.
Urban MW, Pislaru C, Nenadic IZ, Kinnick RR, James F. Measurement of viscoelastic properties of *in vivo* swine myocardium using Lamb Wave Dispersion Ultrasound Vibrometry (LDUV). IEEE Trans Med Imaging 2013;32:247–261.
Vejdani-jahromi M, Nagle M, Trahey GE, Wolf PD. Ultrasound shear wave elasticity imaging quantifies coronary perfusion pressure effect on cardiac compliance. IEEE Trans Med Imaging 2015;34:465–473.
Villemain O, Correia M, Mousseaux E, Baranger J, Zarka S, Podetti I, Soulat G, Damy T, Hagège A, Tanter M, Pernot M, Messas E. Myocardial stiffness evaluation using noninvasive shear wave imaging in healthy and hypertrophic cardiomyopathic adults. JACC Cardiovasc Imaging 2019;12:1135–1145.
Voigt JU. Direct stiffness measurements by echocardiography. Does the search for the holy grail come to an end? JACC Cardiovasc Imaging 2019;12:1146–1148.
Vos HJ, van Dalen BM, Heinonen I, Bosch JG, Sorop O, Duncker DJ, van der Steen AFW, de Jong N. Cardiac shear wave velocity detection in the porcine heart. Ultrasound Med Biol 2017;43:753–764.
Wassenaar PA, Eleswarpu CN, Schroeder SA, Mo X, Raterman BD, White RD, Kolipaka A. Measuring age-dependent myocardial stiffness across the cardiac cycle using MR elastography: A reproducibility study. Magn Reson Med 2016;75:1586–1593.
Xu K, Laugier P, Minonzio J-G. Dispersive Radon transform. J Acoust Soc Am 2018;143:2729–2743.